Energy-Resolved SEU Cross Section From 10-meV to 800-MeV Neutrons by Time-of-Flight Measurement

Hidenori Iwashita, Ryu Kiuchi, Yoshiharu Hiroshima, Yuichiro Okugawa, Tomoki Sebe, Miki Takeda, Hirotaka Sato, Takashi Kamiyama, Michihiro Furusaka, and Yoshiaki Kiyanagi

***Abstract*— We performed continuous observations of single-event upset (SEU) cross sections for the energy range of 10 meV–1 MeV at the Japan Proton Accelerator Research Complex (J-PARC). As a result, we were able to clearly observe the effect on the cross section of the ^{10}B(n, α)^{7}Li reaction below 0.1 MeV.**

***Index Terms*— Field-programmable gate arrays (FPGAs), neutron energy-dependent radiation effects, particle accelerator, single-event upset (SEU) cross section, time-of-flight (TOF) technique.**

I. Introduction

MODERN society's various infrastructures are becoming increasingly dependent on digital technologies and are undergoing a digital transformation [1], [2]. However, although this enables people to enjoy greater convenience in their everyday lives, various issues, such as software bugs in electronic device logic and compromised security, have become major social problems [3]. In addition, random phenomena called bit errors can occur in semiconductor devices such as large-scale integrated circuits (LSIs), including memory chips. Soft errors caused by cosmic rays are one category [4], but there are many cases where the causes are unknown [5], making them very difficult problems to solve. At present, neutrons generated by cosmic rays are considered to be one of the main causes of soft errors in semiconductor devices in electronic equipment used on the ground [6], [7], and [8].

It is therefore crucial to design and fabricate semiconductor devices and systems so as to minimize the single-event upset (SEU) error rate measured in failure in time (FIT) units and thus to ensure the reliability and safety of these devices and systems. In order to calculate the expected number of failures due to soft errors in various neutron environments (ground, building, accelerator facility, nuclear plant, underground, space, and so on), the number of neutrons per unit time at each neutron energy and the SEU cross section at this energy are required for a wide energy range of neutrons impinging on a particular target [9]. The SEU cross section $\sigma_{\mathrm{SEU}}(E_{\mathrm{n}})$ is defined as

$$\sigma_{\mathrm{SEU}}(E_{\mathrm{n}}) = \frac{N_{\mathrm{SEU}}(E_{\mathrm{n}})}{\Phi(E_{\mathrm{n}})} \tag{1}$$

which identifies a neutron fluence $\Phi(E_{\mathrm{n}})$ as the total number of neutrons per unit area impinging on the semiconductor device and the total number of SEUs, $N_{\mathrm{SEU}}(E_{\mathrm{n}})$, generated by these neutrons. Specifically, it indicates the probability that one neutron per unit area causes soft errors. Note that the SEU cross section for each neutron energy will differ for each semiconductor device. In addition, neutrons in the natural environment and neutrons generated by accelerators have different energy distributions. Therefore, the soft-error rate (SER) in a specific neutron irradiation environment can be indicated as

$$\mathrm{SEU} = \int_0^\infty \sigma_{\mathrm{SEU}}(E_{\mathrm{n}})\phi(E_{\mathrm{n}})dE_{\mathrm{n}} \tag{2}$$

using the neutron flux $\phi(E_{\mathrm{n}})$ (the number of neutrons with energy E_{n} crossing a unit area in a unit time) at each neutron energy E_{n} and SEU cross section $\sigma_{\mathrm{SEU}}(E_{\mathrm{n}})$. Thus, the SEU cross section is the most important basic data point that is necessary for calculating the failure rate of semiconductor devices due to soft errors.

Therefore, we devised a new method for measuring the energy dependence of a neutron-induced SEU cross section for a field-programmable gate array (FPGA) using the neutron time-of-flight (TOF) technique up to 800 MeV. Using this method, we were able to measure the SEU cross section with high energy resolution from 1 to 800 MeV at the ICE House of Los Alamos Neutron Science Center (LANSCE) [10]. However, it is impossible to measure the neutron energy range below 1 MeV at the LANSCE radiation effects facilities, ICE House and ICE II, because the interval repetition of the proton beam, which is produced as a pulsed neutron beam, is 1.8 μs

Manuscript received 3 January 2023; revised 8 February 2023; accepted 9 February 2023. Date of publication 15 February 2023; date of current version 15 March 2023.

Hidenori Iwashita, Ryu Kiuchi, Yoshiharu Hiroshima, and Yuichiro Okugawa are with Nippon Telegraph and Telephone Corporation (NTT), Tokyo 180-8585, Japan (e-mail: hidenori.iwashita.ux@hco.ntt.co.jp).

Tomoki Sebe, Miki Takeda, Hirotaka Sato, Takashi Kamiyama, and Yoshiaki Kiyanagi are with the Faculty of Engineering, Hokkaido University, Sapporo 060-8628, Japan.

Michihiro Furusaka is with the Faculty of Engineering, Hokkaido University, Sapporo 060-8628, Japan, also with the National Institute of Advanced Industrial Science and Technology, Tsukuba 305-8568, Japan, and also with the High Energy Accelerator Research Organization, Tsukuba 305-0801, Japan.

Color versions of one or more figures in this article are available at https://doi.org/10.1109/TNS.2023.3245142.

Digital Object Identifier 10.1109/TNS.2023.3245142

(1.8 μs corresponds to the neutron flight time of 0.6-MeV neutrons over a neutron flight path length of 20 m) and the neutron intensity below 1 MeV is very low. The JESD89B standard defines a test method for determining a thermal neutron SEU cross section using a nuclear reactor or an accelerator-driven neutron source with moderators [9]. In this method, the thermal neutron SEU cross section is calculated by subtracting the total (high energy plus thermal neutron) SEU cross section measured without a thermal neutron shield from the high-energy SEU cross section measured with the thermal neutron shield. Therefore, since continuous neutron energy dependence cannot be measured, the thermal neutron SER in terrestrial can be accurately calculated only when the neutron spectral shapes in terrestrial and the accelerated tests are almost identical. It is a serious defect for both scientific studies and industrial applications that neutron energy-dependent SEU cross sections below 1 MeV with high resolution are not measured since thermal neutrons vary greatly depending on the moisture content of the atmosphere and the hydrogen-containing materials surrounding semiconductors. Note that there have been many studies on thermal neutron-induced soft errors, and the thermal neutron SEU cross section has already been measured using nuclear reactors and accelerator-driven neutron sources [11], [12], [13], [14], [15], [16], [17], [18], [19], [20]. In a recent report on 2021, for most of the devices, SER in terrestrial was dominated by high-energy neutrons, with thermal neutrons contributing as low as 1%, but there was one device with thermal neutrons contribution exceeding 10% [18]. There are also reports that SEUs due to thermal neutrons occur even in modern devices without borophosphosilicate glass (BPSG). If the SEU cross section of a sufficiently wide energy range is unknown, accurate soft-error rates cannot be evaluated for various neutron fields.

The pulsed neutron source at materials and life science experimental facility (MLF) in the Japan Proton Accelerator Research Complex (J-PARC) has high neutron intensity below 1 MeV. Therefore, we decided to use the facility at J-PARC MLF to perform a continuous measurement of an energy-dependent neutron-induced SEU cross section for an energy range extending below 1 MeV. Here, we present the results obtained at neutron energies less than 1 MeV and discuss the overall cross section from 10 meV to 800 MeV.

II. Measurement Methods

A. TOF Technique

The TOF technique makes it possible to determine neutron velocity v (i.e., neutron kinetic energy) by measuring the flight time of a neutron along a known path length. In the sub-GeV region, neutrons have velocities close to the speed of light, and thus, we need to consider relativistic effects. The neutron energy E_{n} is determined from

$$E_{\mathrm{n}} = \frac{m_0c^2}{\sqrt{1-\frac{v}{c}}}^2 - m_0c^2 = \frac{m_0c^2}{\sqrt{1-\frac{v}{ct}}}^2 - m_0c^2 \tag{3}$$

where m_0 is the neutron rest mass, v is its velocity, c is the speed of light, L is the flight path length, and t is the neutron flight time. Using the TOF technique, it is possible to determine the energy of the neutron that caused a soft error by measuring the time when the soft error occurred. The relationship between the TOF at $L = 13.7$ m and the neutron energy is shown in Fig. 1.

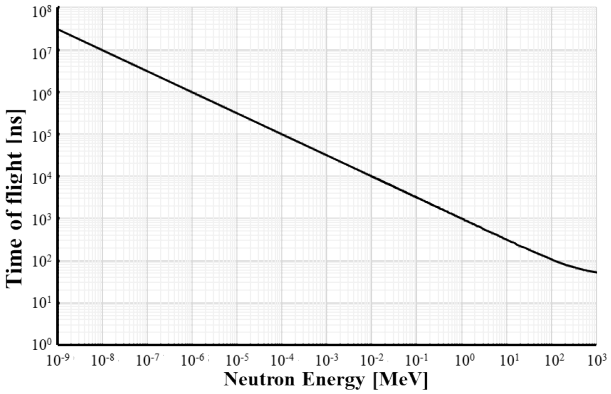

Fig. 1. Neutron energy versus the TOF at $L = 13.7$ m. The neutron energy E_{n} is determined from (3).

B. Soft-Error Detection on a Nanosecond Scale Using FPGAs

In addition, in this experiment, we used the high-speed soft-error detection circuit that we had previously developed for the experiment at LANSCE [10]. The circuit can identify, in the order of nanoseconds, the energy of the neutron that causes a soft error by detecting a logical malfunction that occurs in the configuration random access memory (CRAM) of an FPGA. However, not all soft errors that occur in CRAM are logical malfunctions, so the CRAM bit error rate and logical malfunction rate are different. On the other hand, the functioning of a CRAM cyclic redundancy check (CRC) check is such that it can detect all CRAM bit errors. Moreover, the energy-dependent probability distributions of the logical malfunction and the CRAM error are identical since the CRAM error causes the logical malfunction. These relationships can be defined by

$$P_{\mathrm{CRAM}}(E) = P_{\mathrm{LM}}(E) = \frac{N_{\mathrm{CRAM}}(E)}{N_{\mathrm{CRAM}}} = \frac{N_{\mathrm{LM}}(E)}{N_{\mathrm{LM}}} \tag{4}$$

where $P_{\mathrm{CRAM}}(E)$ is the probability distribution of the number of CRAM errors as a function of neutron energy; $P_{\mathrm{LM}}(E)$ is the probability distribution of the number of logical malfunctions as a function of neutron energy; $N_{\mathrm{CRAM}}(E)$ and $N_{\mathrm{LM}}(E)$ are the CRAM errors, where the logical malfunction counts as a function of E; and N_{CRAM} and N_{LM} are the CRAM errors, where the logical malfunction counts for the whole energy range ($N_{\mathrm{CRAM/LM}} = \int N_{\mathrm{CRAM/LM}}(E)dE$).

Therefore, the CRAM error cross section depending on the neutron energy, $\sigma_c(E)$, is given as

$$\sigma_c(E) = \frac{N_{\mathrm{CRAM}}(E)}{\phi(E)} = \frac{N_{\mathrm{CRAM}} \times P_{\mathrm{LM}}}{\phi(E)} \tag{5}$$

where $\phi(E)$ is the spectral neutron fluence to which the device was exposed in units of n/cm^2/MeV. It is difficult to measure the logical malfunction as a function of the flight time, $P_{\mathrm{LM}}(E)$, and the CRAM error rate, N_{CRAM}, at the

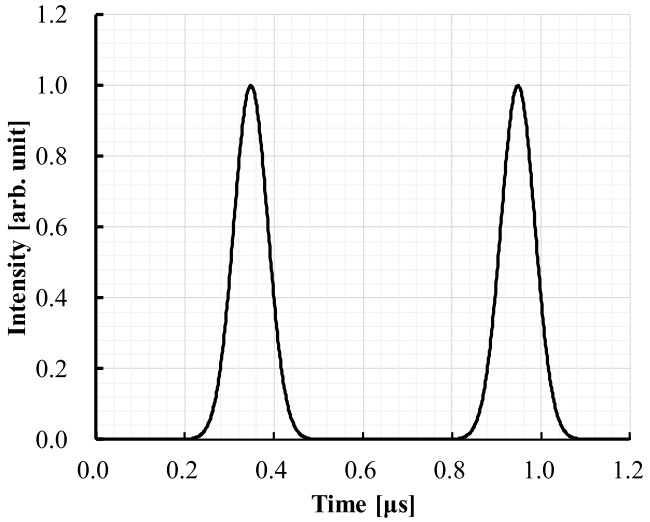

Fig. 2. Time structure of proton pulse at J-PARC (200 kW) [22]. The proton pulse of this facility is double bunch with a peak-to-peak measurement of 600 ns.

same time because the logical malfunction is recovered by reconfiguration or by turning the power back on. For this reason, we measured $P_{\mathrm{LM}}(E)$ first and then N_{CRAM}. Note that this circuit cannot distinguish the difference between single-bit and multibit errors.

We adopted this method that can detect soft errors within nanosecond order to measure wide neutron energy range from 10 meV to several hundred MeV at J-PARC. Note that for measurements in the low-energy regions only, it may be more efficient to measure the TOF of SEUs in the block random access memory (BRAM) of the FPGA than with this method using the CRAM. Because the BRAM measurement is high detection efficiency and does not need to be measured in two steps, the measurement may be simpler and more efficient.

C. Facilities

We conducted experiments using the neutron beamline for observation and research use (NOBORU) instrument at No. 10 beamline (BL10) in J-PARC MLF [21]. MLF has 23 neutron beam ports and 21 neutron instruments in operation. NOBORU was constructed for use in various new experiments and for the characterization of neutron source performance since beamline neutron characteristics are highly requested. NOBORU has an experimental room with a dimension of 3 (W) $\times$ 4 (L) $\times$ 2 (H) m^3 surrounded by shielding walls made of steel and concrete. A neutron beam with 10 $\times$ 10 cm^2 cross section is produced for the experiments. NOBORU has several optical devices to control neutron intensity, neutron beam shape, and energy spectrum based on the requirements of each experiment.

Fig. 2 shows the fit curve of the measured time structure of the proton pulse at an accelerator power of 200 kW [22]. As can be seen, the energy resolution of measurements in the high-energy region above about 0.1 MeV is not very high since the proton pulse of this facility is double-bunch with a peak-to-peak measurement of 600 ns.

Fig. 3 shows the calculated neutron spectrum intensity at 13.4 m from the moderator surface in BL10 using the

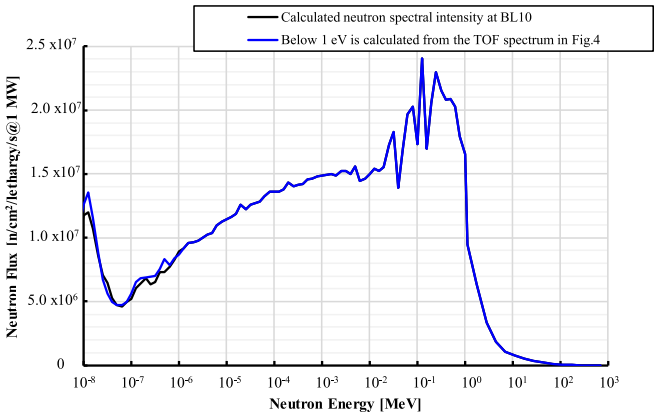

Fig. 3. Neutron spectral intensities at BL10 at accelerator power of 1 MW [21]. The black line is calculated neutron spectral intensity at 13.4 m from the moderator surface using the PHITS code [23] and JENDL-3.2 [21], [24]. The blue line is the neutron energy spectrum at $L = 13.7$ m and the spectrum below 1 eV is calculated from the TOF spectrum in Fig. 4.

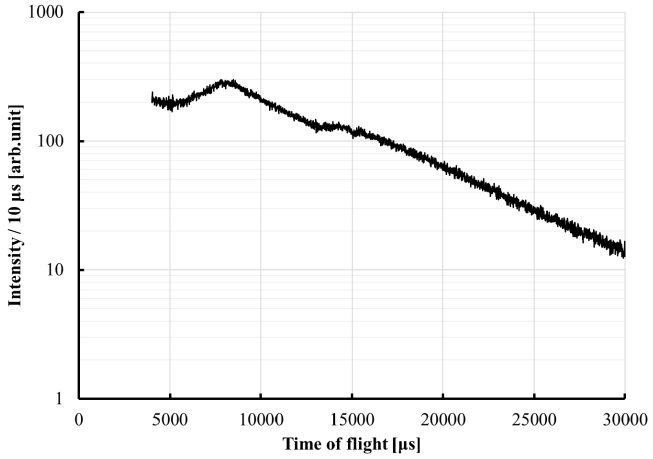

Fig. 4. TOF spectrum at BL10 measured by Dr. M. Harada. These data were used to calculate the relative values of the cross section at a neutron energy below 20 eV.

particle and heavy ion transport code system (PHITS) code [23] and JENDL-3.2 [21], [24]. This simulation is precisely reproduced the geometry and materials of the beamline around devices under test (DUTs) [25]. The adequacy of the calculated spectrum is confirmed using the foil activation method. Fig. 4 shows the TOF spectrum measured by Dr. M. Harada, an instrument scientist of the NOBORU instrument. These data can be used to correct the shape of the low-energy neutron spectrum below 20 eV.

III. Experiment

We performed the experiment at a proton beam power of 790 kW. The irradiated DUTs were two types of commercially available FPGA with design rules of 40 and 55 nm. We made separate measurements of logical malfunctions as a function of neutron energy and CRAM error counts for the whole energy range. The experimental setup at BL10 NOBORU is shown in Fig. 5. This beamline has various neutron and γ-ray filters and neutron collimators that can be applied between the beam ducts, but we did not use them. The DUTs were installed at a distance of 13.7 m from the moderator.

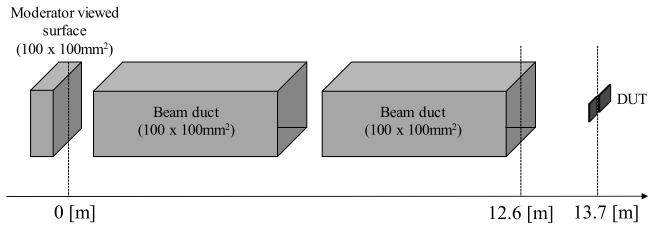

Fig. 5. Our experimental setup at BL10. We did not use neutron/γ-ray filters or neutron collimators between the beam ducts. The DUTs were installed at a distance of 13.7 m from the moderator.

For the measurement of logical malfunctions, the DUTs and the controller board are connected to provide four signals (error, status, reconfiguration, and power). The error signal is a timing signal indicating the point at which a logical malfunction is detected. The status signal indicates the status of the DUT during startup, monitoring, and error occurrence. The reconfiguration signal is for reconfiguring the FPGA in the DUT from the controller board. The power signal controls the power supply of the FPGA in the DUT from the controller board. The DUTs are recovered after an error by reconfiguring or restarting the FPGA power supply. The reconfiguration time is 300 ms for FPGA 40 nm and 10 ms for FPGA 55 nm. Power OFF and ON is executed when reconfiguration does not recover. First, the OFF time is 1 s, and when it still does not recover, the time is gradually increased to 5, 10, and then 20 s to recover. The controller board calculates the time difference between the proton pulse and the error signal and performs recovery control of the DUTs. An FPGA of the controller board located 20 cm from the DUTs is reconfigured when a soft error occurs. Also, the controller board outputs the time difference value to a PC.

For the measurement of CRAM error counts for the whole energy range, the CRC function of the FPGA was used to detect CRAM errors. The CRC value is calculated when generating the configuration bitstream [26], [27], [28]. After the configuration bitstream is loaded into the FPGA, the CRC circuit of the FPGA calculates the CRC value of the CRAM and compares it with the precalculated CRC value. When a soft error occurs in the CRAM, the CRC values become inconsistent, and the error can be detected.

IV. Results

The results of TOF spectra of the logical malfunction counts for the two FPGAs are shown in Fig. 6. Fig. 6(a) clearly shows the double pulse structure. However, we were not able to deduce the cross section from this since the pulsewidth of each proton pulse was about 100 ns, and then, the energy resolution was very poor. Fig. 6(b) indicates that logical malfunctions occurred even at large flight time values and low energy. The total counts of logical malfunctions in each FPGA were given as follows: the 40-nm FPGA $=117\ 694$ counts and the 55-nm FPGA $=269\ 227$ counts. One FPGA 40 nm and eight FPGA 55 nm were irradiated at the same time. The average interval of logical malfunctions for FPGA 40 nm and FPGA 55 nm was 1.8 and 6.3 s, respectively. The irradiation time for FPGA 40 nm was 48 h and the

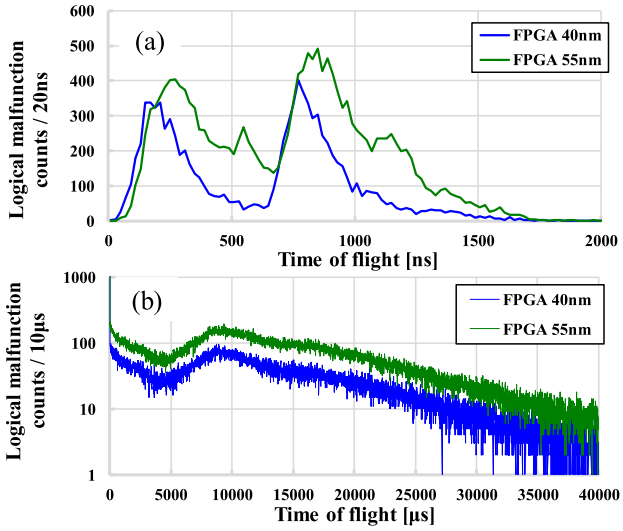

Fig. 6. Results of TOF spectra of logical malfunction counts for the two FPGAs, which were the DUTs. Time bin of (a) 20 ns and (b) 10 μs.

TABLE I
Results of Measurement of N_{CRAM}

Design rule [nm]	Number of protons irradiated to the neutron production target	Irradiation time [second]	CRAM error counts per Mbit (N_{CRAM})
40	1.16×10^{18}	666	37.5
55	8.81×10^{17}	506	30.5

total irradiation time of eight FPGA 55 nm was 474 h. These irradiation times do not include downtimes for reconfiguration and power OFF–ON cycle. If two logical malfunctions occur in one proton shot, the second logical malfunction is not counted. However, such cases are almost negligible because the average intervals of logical malfunction were longer than 1.8 s and proton shots of J-PARC were 25 Hz. In addition, Table I shows a summary of the CRAM error counts with proton shot number and irradiation time. The CRAM capacities of FPGA 40 nm and FPGA 55 nm are 161.6 and 25.6 Mbit, respectively. Also, in the CRAM measurement, one FPGA 40 nm and eight FPGA 55 nm were irradiated at the same time. FPGA 40 nm can distinguish the difference among a single-bit error, a double-adjacent bit error, and uncorrectable errors. As a result, 82.2% were counted as single-bit errors, 5.3% were counted double-adjacent bit errors and 12.5% were counted uncorrectable error. FPGA 55 nm does not have the function to distinguish different errors.

The blue line in Fig. 3 shows the neutron energy spectrum at a proton beam power of 790 kW with $L = 13.7$ m. This spectrum was converted from the calculated spectrum in Fig. 3 for a proton beam power of 790 kW with $L = 13.7$ m. In addition, the spectrum below 1 eV is deduced from the TOF spectrum shown in Fig. 4 by conversion into a neutron energy spectrum.

Fig. 7 shows the CRAM SEU cross section calculated from the measured logical malfunction time distribution, CRAM error counts, and neutron energy spectrum. The vertical error bars are calculated with standard deviation

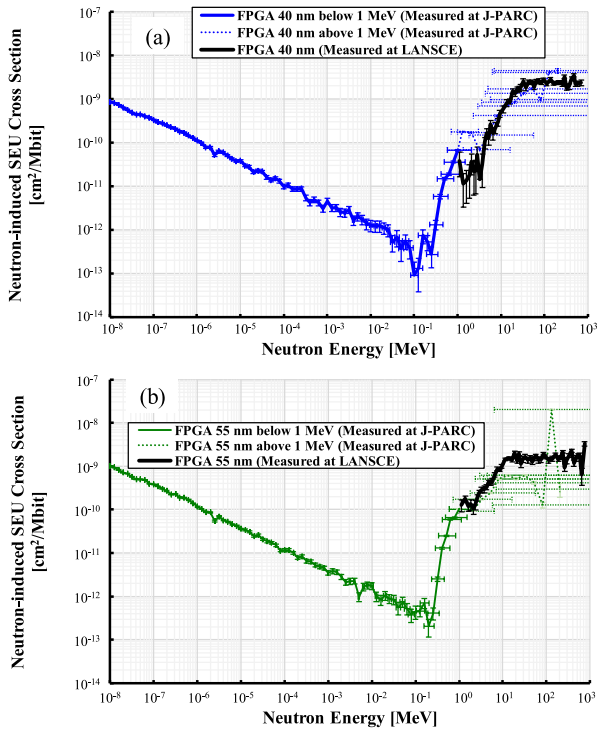

Fig. 7. SEU cross section of (a) FPGA 40 nm and (b) FPGA 55 nm. The SEU cross sections above 0.1 MeV at J-PARC are not accurate because of the double pulse (see Fig. 2).

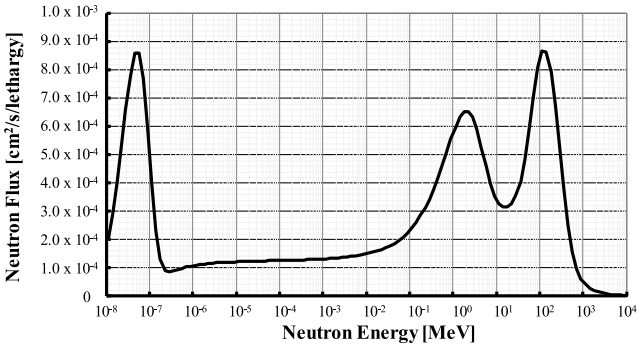

Fig. 8. Spectra of neutron flux at the ground surface calculated by EXPACS [31], [32], [33] under the following conditions: altitude = 0 m, latitude = 35°, longitude = 142°, and moisture content = 0.2.

(1σ: 68% confidence interval). The horizontal error bars are calculated with 600 ns of the peak-to-peak of double-bunch. The SEU cross sections above 0.1 MeV are not accurate because of the double pulse (see Fig. 2).

V. Discussion

We obtained the SEU cross sections continuously over an energy range of 10 meV–800 MeV by combining the results from our TOF experiment at J-PARC and our experiment at LANSCE. The $1/v$ proportionality of the results suggests that the SEU cross section below 0.1 MeV is due to the $^{10}\mathrm{B}(n, \alpha)^{7}\mathrm{Li}$ reaction since its absorption cross section also follows $1/\sqrt{E}$ ($1/v$ law) and this reaction generates charged particles (alpha and Li particles) that are strong causes of SEUs. This trend was anticipated by Cecchetto et al. [29].

TABLE II
Percentage Contribution of Each Energy Range to the SEUs on GroundSurface

Energy region	SER of 40nm FPGA	SER of 55nm FPGA
Below 1 eV	18.24%	26.66%
1 eV to 1 keV	0.56%	0.76%
1 keV to 1 MeV	0.22%	0.56%
1 MeV to 1 GeV	79.61%	69.83%
Above 1 GeV	1.37%	2.19%

Although these devices feature modern components without BPSG, SEU cross sections in the thermal neutron energy region showed similar energy dependence to the boron capture cross section in the experiment reported here.

In addition, the energies of α and ^{7}Li particles produced in all directions by the $^{10}\mathrm{B}(n, \alpha)^{7}\mathrm{Li}$ reaction are 1.4 MeV (α) and 0.82 MeV (^{7}Li). The ranges of these particles in Si are 4 μm (α) and 2 μm (^{7}Li) [30]. These secondary particles do not affect this TOF measurement because they are fast and short ranges enough.

We calculated error rates for various energy regions, and the contribution of each energy region to the total SER was obtained assuming a neutron energy spectrum on a ground surface. Fig. 8 shows a neutron spectrum on a ground surface calculated by excel-based program for calculating atmospheric cosmic-ray spectrum (EXPACS) [31], [32], [33] under the following conditions: altitude = 0 m, latitude = 35°, longitude = 142°, and moisture content = 0.2. Table II shows the percentage contributions of each neutron energy range to the SEUs on the ground surface calculated from the SEU cross sections for the 40- and 55-nm FPGAs. These were calculated from the SEU cross section measured at LANSCE above 1 MeV, from the SEU cross section measured at J-PARC below 1 MeV, and from the SEU cross section for a constant value above 800 MeV. As a result, the contribution of thermal neutrons (below 1 eV) was 18.24% for the 40-nm FPGA and 26.66% for the 55-nm FPGA, and it was clarified that these levels were rather high. These SEU cross sections make it possible to calculate the SERs in the thermal neutron range, which tend to fluctuate depending on the environment.

VI. Conclusion

We measured a neutron-induced SEU cross section for FPGAs using the TOF technique for an energy range from 10 meV to 800 MeV at J-PARC and LANSCE. The effect on the cross section of the $^{10}\mathrm{B}(n, \alpha)^{7}\mathrm{Li}$ reaction was clearly observed below 0.1-MeV neutrons. As a result, it was found that the contribution of low-energy neutrons to soft errors was about 1/5–1/4 of the total error count and 1/4–1/3 with neutrons over 1 MeV, and we believe that these are significant proportions.

Acknowledgment

The neutron experiment at the Japan Proton Accelerator Research Complex (J-PARC) MLF BL10 NOBORU was performed under a user program (Proposal No. 2022A0249). The authors would like to extend their sincere appreciation to

Dr. K. Oikawa and Dr. M. Harada at J-PARC for their support during this experiment, and T. Ikeda, Y. Okazaki, and Y. Maeda of NTT Space Environment and Energy Laboratories for their support in this research.

REFERENCES

[1] E. Stolterman and A. C. Fors, "Information technology and the good life," in *Information Systems Research* (IFIP International Federation for Information Processing), vol. 143. New York, NY, USA: Springer, Jul. 2004, pp. 687–692. [Online]. Available: https://link.springer.com/book/10.1007/b115738

[2] S. Nambisan, M. Wright, and M. Feldman, "The digital transformation of innovation and entrepreneurship: Progress, challenges and key themes," *Res. Policy*, vol. 48, no. 8, Oct. 2019, Art. no. 103773.

[3] World Economic Forum. (Jan. 2020). *The Global Risks Report 2020*. [Online]. Available: https://www.weforum.org/reports/the-global-risks-report-2020

[4] E. Ibe, "Introduction," in *Terrestrial Radiation Effects in ULSI Devices and Electronic Systems*, 1st ed. Hoboken, NJ, USA: Wiley, Mar. 2015, pp. 1–12.

[5] *Overview of Particle Radiation Effects on Telecommunication Systems*, document ITU-T Recommendation K.124, Jan. 2020.

[6] J. F. Ziegler, "Terrestrial cosmic rays," *IBM J. Res. Dev.*, vol. 40, no. 1, pp. 19–39, Jan. 1996.

[7] E. Normand, "Single event upset at ground level," *IEEE Trans. Nucl. Sci.*, vol. 43, no. 6, pp. 2742–2750, Dec. 1996.

[8] G. Hubert and L. Artola, "Experimental evidence of ground albedo neutron impact on soft error rate for nanoscale devices," *IEEE Trans. Nucl. Sci.*, vol. 66, no. 1, pp. 262–269, Jan. 2019.

[9] *Measurement and Reporting of Alpha Particle and Terrestrial Cosmic Ray-Induced Soft Errors in Semiconductor Devices*, JEDEC Standard JESD89B, Sep. 2021.

[10] H. Iwashita et al., "Energy-resolved soft-error rate measurements for 1–800 MeV neutrons by the time-of-flight technique at LANSCE," *IEEE Trans. Nucl. Sci.*, vol. 67, no. 11, pp. 2363–2369, Nov. 2020.

[11] D. Lambert et al., "Single event upsets induced by a few MeV neutrons in SRAMs and FPGAs," in *Proc. IEEE Radiat. Effects Data Workshop (REDW)*, Jul. 2017, pp. 114–118.

[12] G. Hubert and L. Artola, "Study of secondary scattering/albedo neutron fields and their impacts on SER as function of scene topologies," *IEEE Trans. Nucl. Sci.*, vol. 67, no. 1, pp. 201–209, Jan. 2020.

[13] J. L. Autran, S. Serre, S. Semikh, D. Munteanu, G. Gasiot, and P. Roche, "Soft-error rate induced by thermal and low energy neutrons in 40 nm SRAMs," *IEEE Trans. Nucl. Sci.*, vol. 59, no. 6, pp. 2658–2665, Dec. 2012.

[14] T. Yamazaki et al., "Origin analysis of thermal neutron soft error rate at nanometer scale," *J. Vac. Sci. Technol. B, Nanotechnol. Microelectron., Mater., Process., Meas., Phenomena*, vol. 33, no. 2, Mar. 2015, Art. no. 020604.

[15] Y.-P. Fang and A. S. Oates, "Thermal neutron-induced soft errors in advanced memory and logic devices," *IEEE Trans. Device Mater. Rel.*, vol. 14, no. 1, pp. 583–586, Mar. 2014.

[16] G. Tsiligiannis et al., "Radiation effects on deep submicrometer SRAM-based FPGAs under the CERN mixed-field radiation environment," *IEEE Trans. Nucl. Sci.*, vol. 65, no. 8, pp. 1511–1518, Aug. 2018.

[17] E. C. Auden et al., "Thermal neutron-induced single-event upsets in microcontrollers containing boron-10," *IEEE Trans. Nucl. Sci.*, vol. 67, no. 1, pp. 29–37, Jan. 2020.

[18] A. Coronetti et al., "Thermal-to-high-energy neutron SEU characterization of commercial SRAMs," in *Proc. IEEE Nucl. Space Radiat. Effects Conf. (NSREC)*, Jul. 2021, pp. 32–36.

[19] E. Normand, K. Vranish, A. Sheets, M. Stitt, and R. Kim, "Quantifying the double-sided neutron SEU threat, from low energy (thermal) and high energy (>10 MeV) neutrons," *IEEE Trans. Nucl. Sci.*, vol. 53, no. 6, pp. 3587–3595, Dec. 2006.

[20] J. Park et al., "Development of thermal neutron SER-resilient high-*k*/metal gate technology," in *Proc. IEEE Int. Rel. Phys. Symp.*, Jun. 2014, pp. 2B.4.1–2B.4.3.

[21] M. Harada, M. Teshigawara, M. Ooi, K. Oikawa, H. Takada, and Y. Ikeda, "Experimental characterization of high-energy component in extracted pulsed neutrons at the J-PARC spallation neutron source," *Nucl. Instrum. Methods Phys. Res. A, Accel. Spectrom. Detect. Assoc. Equip.*, vol. 1000, Jun. 2021, Art. no. 165252.

[22] H. Hasemi et al., "Evaluation of nuclide density by neutron resonance transmission at the NOBORU instrument in J-PARC/MLF," *Nucl. Instrum. Methods Phys. Res. A, Accel. Spectrom. Detect. Assoc. Equip.*, vol. 773, pp. 137–149, Feb. 2015.

[23] T. Sato et al., "Features of particle and heavy ion transport code system (PHITS) version 3.02," *J. Nucl. Sci. Technol*, vol. 55, no. 6, pp. 684–690, Jan. 2018.

[24] T. Nakagawa et al., "Japanese evaluated nuclear data library version 3 revision-2: JENDL-3.2," *J. Nucl. Sci. Technol.*, vol. 32, no. 12, pp. 1259–1271, Dec. 1995.

[25] M. Harada, F. Maekawa, K. Oikawa, S.-I. Meigo, H. Takada, and M. Futakawa, "Application and validation of particle transport code PHITS in design of J-PARC 1 MW spallation neutron source," *Prog. Nucl. Sci. Technol.*, vol. 2, pp. 872–878, Oct. 2011.

[26] *Soft Error Measures for Field Programmable Gate Arrays*, document ITU-T Recommendation K.131 Supplement 11, Sep. 2018.

[27] Xilinx Corporation. (May 2018). *Soft Error Mitigation Controller V4.1 LogiCORE IP Product Guide*. [Online]. Available: https://www.xilinx.com/support/documentation/ip_documentation/sem/v4_1/pg036_sem.pdf

[28] Intel Corporation. (Aug. 2019). *AN 539: Test Methodology of Error Detection and Recovery Using CRC in Intel FPGA Devices*. [Online]. Available: https://www.intel.com/content/dam/www/programmable/us/en/pdfs/literature/an/an539.pdf

[29] M. Cecchetto, R. G. Alía, S. Gerardin, M. Brugger, A. Infantino, and S. Danzeca, "Impact of thermal and intermediate energy neutrons on SRAM SEE rates in the LHC accelerator," *IEEE Trans. Nucl. Sci.*, vol. 65, no. 8, pp. 1800–1806, Aug. 2018.

[30] E. Ibe, "Fundamentals of radiation effects," in *Terrestrial Radiation Effects in ULSI Devices and Electronic Systems*. Hoboken, NJ, USA: Wiley, Mar. 2015, pp. 33–48.

[31] T. Sato, "Analytical model for estimating the zenith angle dependence of terrestrial cosmic ray fluxes," *PLoS ONE*, vol. 11, no. 8, Aug. 2016, Art. no. e0160390.

[32] T. Sato, "Analytical model for estimating terrestrial cosmic ray fluxes nearly anytime and anywhere in the world: Extension of PARMA/EXPACS," *PLoS ONE*, vol. 10, no. 12, Dec. 2015, Art. no. e0144679.

[33] JAEA. (Jun. 2022). *Excel-Based Program for Calculating Atmospheric Cosmic-Ray Spectrum*. [Online]. Available: http://phits.jaea.go.jp/expacs/